

# Modeling the mechanical properties of ultra-thin polymer films

Francisco Espinosa-Loza, Michael Stadermann, Chantel Aracne-Ruddle, Rebecca Casey, Philip Miller, and Russel Whitesides

Lawrence Livermore National Laboratory, 7000 East Avenue, L-471, Livermore, CA 94550, USA

(Received 3 November 2016; revised 17 August 2017; accepted 30 August 2017)

## Abstract

A modeling method to extract the mechanical properties of ultra-thin films (10–100 nm thick) from experimental data generated by indentation of freestanding circular films using a spherical indenter is presented. The relationship between the mechanical properties of the film and experimental parameters including load, and deflection are discussed in the context of a constitutive material model, test variables, and analytical approaches. Elastic and plastic regimes are identified by comparison of finite element simulation and experimental data.

**Keywords:** indentation; optimization; ultra-thin films

## 1. Introduction

Freestanding ultra-thin polymer films are utilized in a variety of applications, including sensors, catalysis, filtration, and tissue engineering<sup>[1–4]</sup>. At the National Ignition Facility (NIF), nanometer scale polyvinyl formal films are routinely used as load-bearing elements to support fuel capsules in complex millimeter-scale inertial confinement fusion (ICF) targets<sup>[5]</sup>. Since even very thin films appear to introduce significant perturbation to the implosion<sup>[6, 7]</sup>, there is an impetus to minimize the thickness of such support films. To make certain that thinner films can withstand the rigors of target assembly and handling, their mechanical properties must be well understood.

The mechanical properties of ultra-thin films are known to change as the film dimensions approach the molecular size scales<sup>[8–10]</sup>. Measuring these properties has been difficult even for substrate-supported thin films, and there are only a few measurements that have been attempted on freestanding films<sup>[11]</sup>.

Here, we utilize indentation<sup>[12, 13]</sup> to characterize mechanical properties of such thin films. Closed-form expressions<sup>[14, 15]</sup> for interpreting data gathered from this method have been derived, but such approximations typically perform poorly for pre-stressed films or tests that extend beyond the elastic regime of the polymer. We present a method that can be used to extract mechanical data from such tests and construct full stress–strain curves for films of this

thickness regime. Finite element analysis is used to simulate the indentation test, and an optimization algorithm is used to derive the constitutive material models.

## 2. Experimental

### 2.1. Preparation of the thin films

Freestanding polyvinyl formal films with a thickness of 10–100 nm were made by a spin coating method, as described in detail elsewhere<sup>[16, 17]</sup>. In brief, a solution of 0.25 wt% Vinylec E (SPI Supplies, West Chester, PA) in ethyl lactate (98%, Sigma-Aldrich, St. Louis, MO) was spin coated onto Si wafers pretreated with polydiallyldimethylammonium chloride PDAC (Sigma-Aldrich St. Louis, MO.  $M_w \sim 1 \times 10^5$ – $2 \times 10^5$  g/mol), and baked for 1 min at 50 °C on a hot plate. The resultant films were then lifted from the wafer, in water, and mounted on ring-shaped holders with an inner diameter of 11 mm. The films were typically dried overnight under ambient conditions before being tested using the indentation method. Prior to testing, the thickness of each film was measured by ellipsometry (Woollam M-2000). Since the hydrated polymer swells the films, as mounted on the holders for testing, typically have significant residual stress.

### 2.2. Indentation test

Indentation tests are conducted on the film using a custom-built system as shown in Figure 1(a); the film is glued

Correspondence to: M. Stadermann, 7000 East Ave Livermore, CA 94550. Email: [stadermann2@llnl.gov](mailto:stadermann2@llnl.gov)

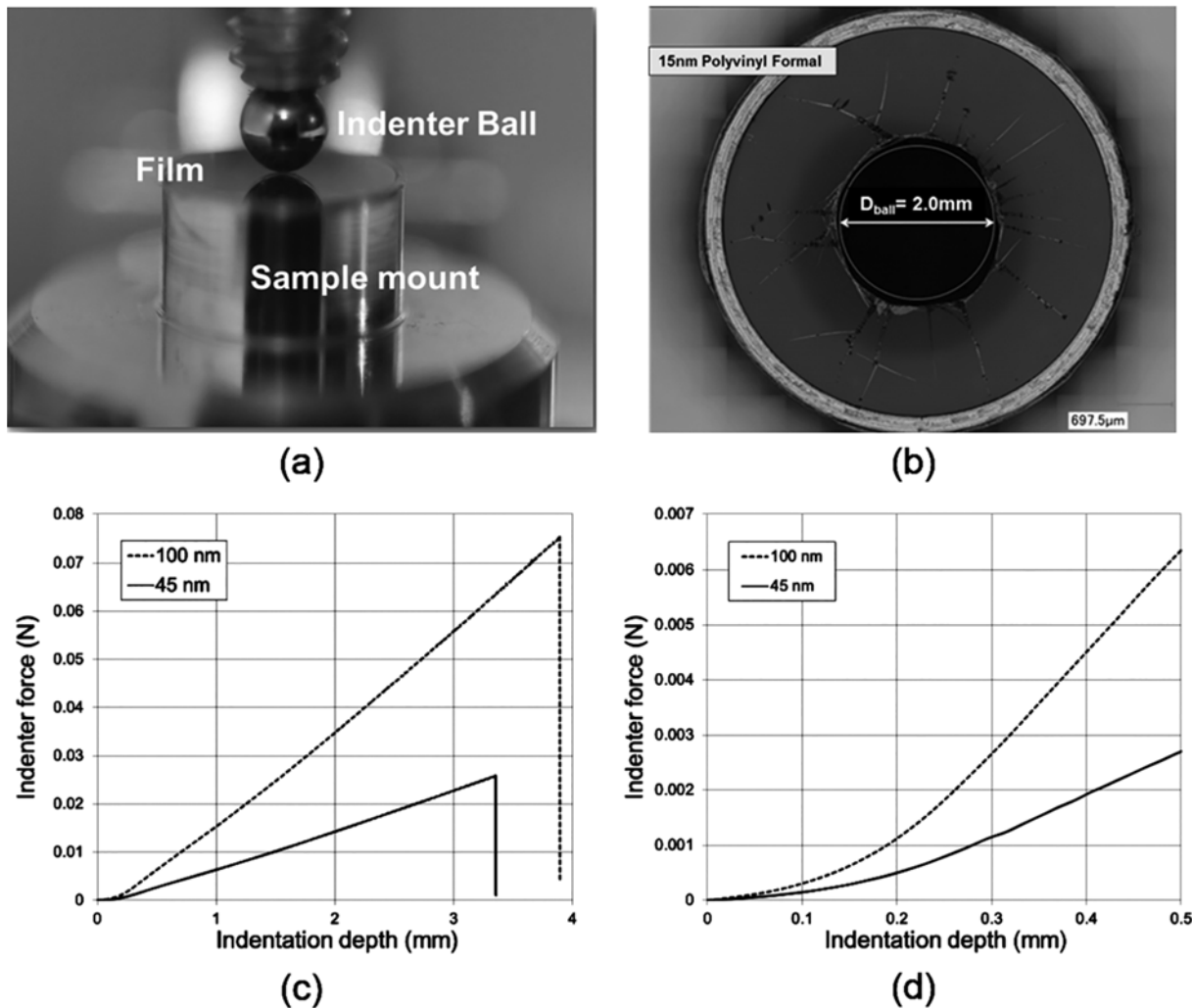


**Figure 1.** (a) Indentation test setup consisting of the film mounted onto a sample holder and the indenter ball on a threaded rod, (b) composite photomicrograph of a typical 15 nm polyvinyl formal film following indentation testing to failure. Note the presence of both circumferential and tangential folds suggesting radial and hoop stress induced deformation during loading. The presence and size of the circumferential rupture indicates the predominance of the radial stress state along the contact radius of the indenter, (c) typical curves for ball indenter test showing failure point. The early curve (d) has an almost cubic shape, while the larger indentation depths show an almost linear response.

onto a 5 mm diameter cylindrical mount and placed on a microbalance (Mettler Toledo MW-124 Weighing Module). A 2 mm sapphire ball attached to a stepper motor (Newport) via leadscrew assembly is used as the indenter. As the film is indented, typically to failure, the load is recorded as a function of the distance that the ball has been pushed into the film (indentation depth  $\delta$ ). Typically, the humidity of the test cell is maintained at 45% relative humidity by means of a water bubbler and two mass flow controllers (MKS Instruments Andover, MA) which are used to adjust the humidity. The indentation method has previously been shown to be suitable for measuring the mechanical properties of even very thin freestanding films<sup>[13]</sup>. Figure 1(c) shows typical force versus indentation depth curves. The film adheres strongly to the indenter ball upon contact; if the ball is withdrawn after an indentation with low depth, it will

pull the film with it far past the initial contact depth. This behavior is also visible in Figure 1(b) where the area in the center of the film that makes contact to the ball is torn out after indentation, showing that adhesion to the ball is stronger than the cohesion of the film. We therefore conclude that there is negligible relative motion (slippage) between film and indenter ball during the test.

### 2.3. Numerical approach

#### 2.3.1. Finite element simulation for indentation test

Finite element simulation of the freestanding film was performed in the finite element software ANSYS Mechanical (Cannonsburg, PA) APDL Release 16.0. An axisymmetric model was created for this analysis. The indenter ball was modeled as a rigid circular target TARGE169 element.

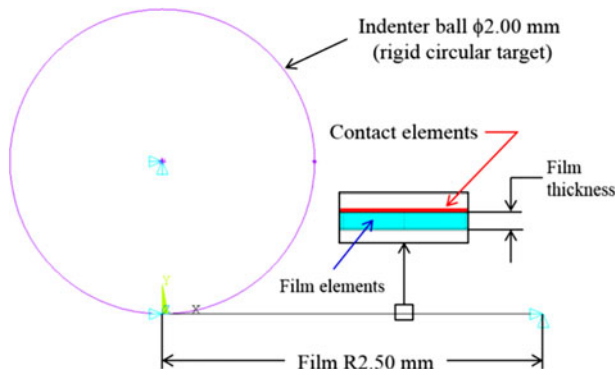


**Figure 2.** Axisymmetric finite element model for indentation test, general dimensions of film and indenter ball.

This element is used to represent various two dimensional (2D) target surfaces for the associated contact element CONTA171. The contact elements themselves overlay the solid elements describing the boundary of a deformable body and are potentially in contact with the target surface, defined by TARGE169. Due the nature of the indentation test, a rough contact behavior was chosen, reflecting the high coefficient of friction between the film and the ball. The film was modeled using a PLANE182, and this 2D 4-Node Structural solid is used for 2D modeling of solid structures. The element can be used as either a plane element (plane stress, plane strain or generalized plane strain) or an axisymmetric element, which is how it is used in this case. It is defined by four nodes having two degrees of freedom at each node: translations in the nodal  $x$  and  $y$  directions. The element has plasticity, hyperelasticity, stress stiffening, large deflection, and large strain capabilities. Figure 2 shows the finite element model for the ball indentation test.

The assumed boundary conditions are that a vertical displacement is applied to the rigid circular target (indentation depth), and that radial displacement is not allowed for the rigid circular target. The film is axially constrained on the outer diameter, and it is radially constrained on the centerline. Sensitivity tests have been performed to assess the influence of mesh size in order to ensure the finite element model is accurate with an optimum requirement on computational resources. A pre-strain is imposed on the film due to the shrinking of the film during the drying process.

### 3. Results and discussion

#### 3.1. Elastic solution

Several authors have presented closed-form equations for the elastic regime for spherical indentation of freestanding circular thin films<sup>[12, 14, 15]</sup>. During the simulation process, we found, for our films, that the elastic assumption is valid only for small values of indentation depth (up to

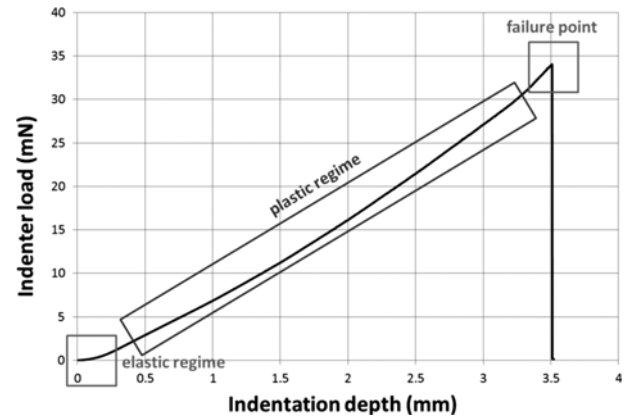


**Figure 3.** Typical experimentally determined material response during an indentation test. The present data was collected for a 100 nm thick polyvinyl formal membrane. Characterized regions of the film material for indentation test.

$\sim 0.200$  mm). Beyond that depth, the mechanical response of the film exhibits plastic deformation until film failure. Figure 3 shows the approximate elastic and plastic regions over the indenter force versus indentation depth curve.

Based on the closed-form approximations given by Begley and Makin<sup>[14]</sup> and experimental data, we computed the elastic modulus for one of our films. Equation (1) shows the deflection of the membrane for the case of zero pre-stretch while Equation (2) includes an initial pre-strain on the membrane.

$$\frac{\delta}{R} = \left(\frac{a}{R}\right)^{3/4} \left(\frac{16}{9\pi} \frac{P}{EhR}\right)^{1/3}, \quad (1)$$

$$\frac{\delta}{R} = \frac{1}{3\pi} \left(\frac{a}{R}\right)^{3/4} \left(\frac{P}{EhR}\right) \left(\frac{1}{\varepsilon_0}\right), \quad (2)$$

where  $\delta$  is the indentation depth or deflection of the membrane,  $R$  is the indenter ball radius,  $a$  is the freestanding radius (span),  $P$  is the indenter load,  $h$  is the film thickness,  $E$  is the elastic modulus of the film,  $\varepsilon_0$  is the pre-strain. For a particular case a 100 nm thick film was chosen. The external diameter of this film is 5 mm, and the ball indenter diameter of 2 mm. Taking a point from the experimental data (Figure 4) at  $\delta = 100 \mu\text{m}$  the corresponding indenter load is  $P = 0.327$  mN; utilizing Equation (1) to compute the elastic modulus we obtain  $E = 14.67$  GPa. Assuming a pre-strain  $\varepsilon_0 = 0.001$  in Equation (2) we obtain an elastic modulus of  $E = 6.96$  GPa.

We then used that value to initialize the simulation. The results are shown in Figure 4. As expected from the original references, the agreement between the closed-form solution and the experimental data is not good for the combination of pre-strain and indentation depth present in our experiments.

In order to improve the agreement between the model and experimental data, it was found necessary to improve our estimate of both the elastic modulus and the pre-strain on

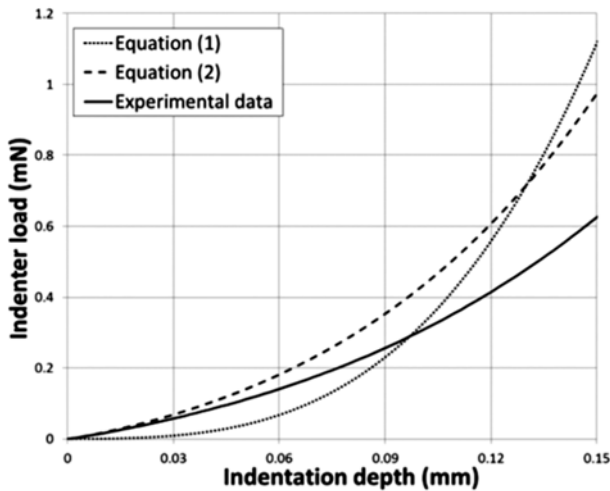


**Figure 4.** Comparison of values derived from a closed-form approximation and experimental indentation data within the elastic portion of the film response. The closed-form approximations, from Ref. [13], were used to estimate a Young's modulus from the indentation data. The resulting modulus was utilized by the elastic model described in Section 2.3.1 of the text. As shown, even within the elastic portion of the curve, there is poor agreement between the computed and the experimental data (solid line).

the film. To do so, an optimization script was written in Python to run ANSYS in batch mode and the Nelder–Mead optimization method was utilized<sup>[18–20]</sup>. In order to extract a unique pair of elastic parameters, Young's modulus  $E$  and pre-strain  $\varepsilon_0$ , the mean square error, defined in Equation (3), the Python script will calculate the error metric shown in Equation (3) for a given  $E$  and  $\varepsilon_0$  and then use the Nelder–Mead optimization method to minimize the error metric:

$$\text{error metric} = \frac{1}{n} \sum_{i=1}^n \sqrt{(F_{\text{num}_i} - F_{\text{exp}_i})^2}, \quad (3)$$

where  $n$  is the number of evaluated nodal points,  $F_{\text{num}_i}$  is the computed indenter load from the finite element analysis at indentation depth  $i$ , and  $F_{\text{exp}_i}$  is the measured indenter load from the experimental data at the corresponding indentation depth  $i$ .

After running the ANSYS simulation with the optimizer to calculate the elastic parameters  $E$  and  $\varepsilon_0$ , good agreement with the experimental data is achieved, as shown in Figure 5.

A sensitivity analysis was conducted to verify that the results of optimized determination of elastic modulus and pre-strain represented an absolute minimum solution space. Multiple simulations were performed to calculate and create the error metric surface plot. Figure 6 shows the results using a 3D surface along with a contour map of such surface, the  $x$ -axis on the contour plot is the elastic modulus, and the  $y$ -axis is the pre-strain of the film.

From Figure 6(a), it is obvious that the pre-strain sensitively affects the fitted value for the modulus. Further, it can be shown that the absolute minimum of the fit depends on the

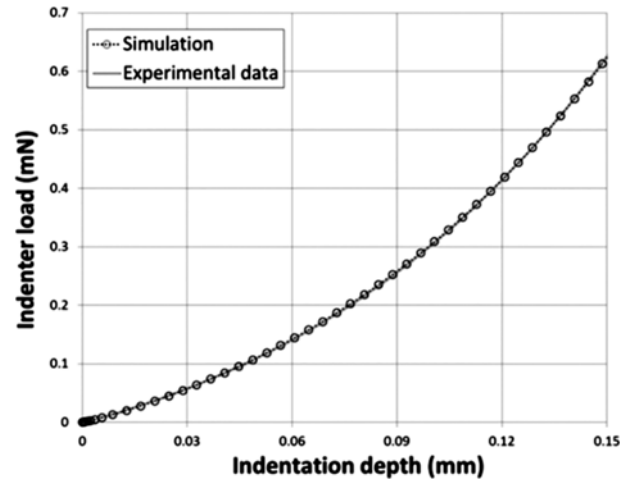


**Figure 5.** Comparison of experimental and the simulated load/displacement response using optimized elastic parameters ( $E$ ). The optimization algorithm was used to extract elastic parameters ( $E = 3.28$  GPa,  $\varepsilon_0 = 0.0018$ ) from the indentation data for a 100 nm thick film. Using these values, modeled and experimental data are in excellent agreement throughout the elastic portion of curve.

range over which the curve is fitted. Figure 6(b) shows the modulus and the error metric as a function of the range over which this curve is fitted. All fits begin with  $x = 0$  mm and end at the indentation depth value. The modulus does not converge toward a number, but increases and then decreases again. We argue that the closest approximation of the fit values to the real values lies at the point where the error metric begins to increase rapidly, around 0.15 mm indentation depth. For an elastic indentation dataset with random noise added to it, the fitted value should converge to the true value for an infinite fit range: at low fit ranges, the noise might cause the fit to find a value that produces a lower error metric than the true value does. As the fit range increases, the fit value will approach the real value while the error metric will approach the measurement accuracy ( $10^{-6}$  N measurement precision). In this case, however, the underlying function transitions from an elastic deformation to a plastic deformation. If the fitted function contains only the elastic part, the error value should increase and the fitted modulus should decrease as the deformation transitions into the plastic regime. Therefore, the point right before the films starts deforming plastically will be the best point to extract the modulus and pre-strain, and that is the point we use for the rest of this work. For this particular film, the error of the modulus starts exceeding  $10^{-6}$  significantly at an indentation depth of 0.170 mm. Due to the scatter in the error, it is not certain at which point exactly the error starts increasing, and the true value could lie between 3.37 GPa (0.15 mm indentation depth) and 3.22 GPa (0.19 mm indentation depth). The spread for the elastic modulus is of the order 0.15 GPa, which we would consider the accuracy of the measurement.

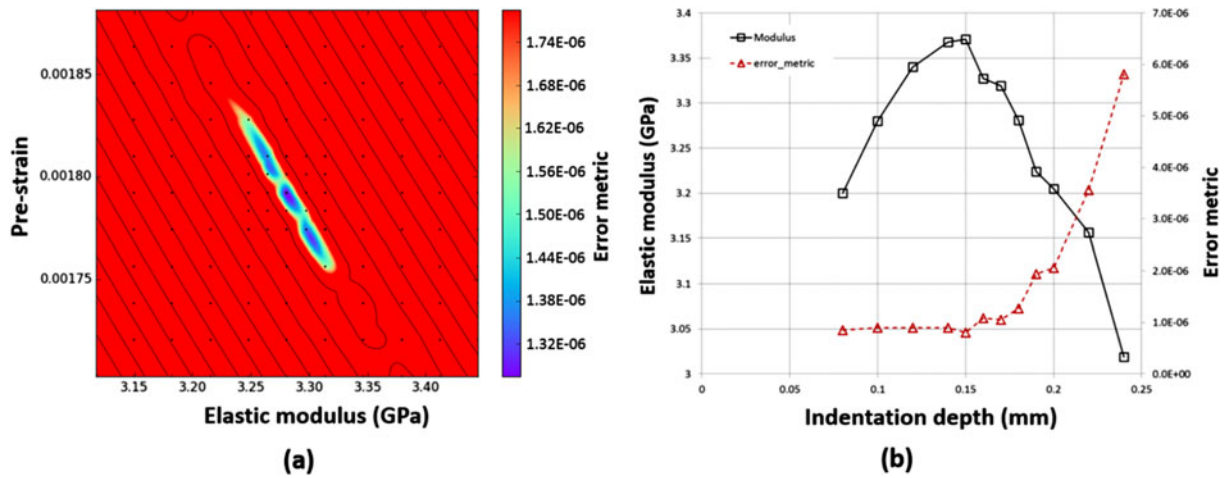


**Figure 6.** (a) Contour plot for the error metric surface generated from indentation simulation shown in Figure 5. A valley of linear combinations of pre-strain and modulus that all come close to satisfying the equation can be seen. (b) Force versus indentation depth (top) and fit values for different indentation depths (bottom). The fit uses all data points from zero to the given depth. The error of the fit stays low until the behavior transitions from elastic to plastic, between 170 and 190  $\mu\text{m}$  of indentation depth, and in this region, the elastic modulus should be read.

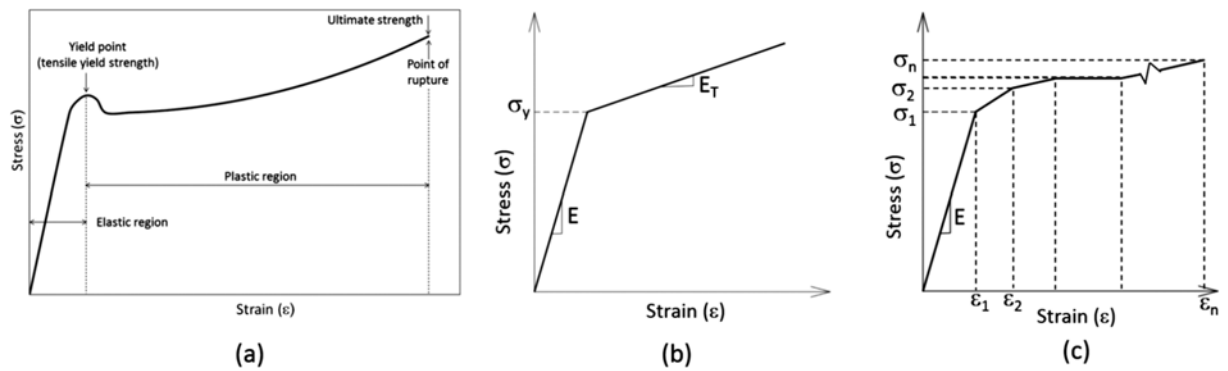


**Figure 7.** (a) Typical stress–strain curve for a polymer. These complex curves can be approximated with two plasticity materials models in ANSYS, and utilized in the present work. (b) Bilinear model. The material response consists of an elastic response, characterized by an elastic modulus ( $E$ ) followed, at a yield point ( $\sigma_y$ ), by a simple plastic response characterized by a tangent modulus ( $E_T$ ). (c) Multilinear model where the material response is described by a series of stress points ( $\sigma_n$ ) and their corresponding strain points ( $\epsilon_n$ ).

### 3.2. Plastic solution

A simple linear elastic model is generally not appropriate for numerical simulations of conformed mechanical components. Such processes have often large permanent deformations, and require material models that account for deviations from elastic (linear) behavior and account for nonlinearities in material response including plastic and/or visco-plastic behavior. Deviations from simple linear behavior are quite evident in the present material system.

In order to construct a high fidelity finite element simulation, a number of important parameters must be considered including mesh quality, solver type, contact behavior, boundary conditions, and the material properties. One of the principal difficulties with finite element modeling is selecting the appropriate properties for the material involved. The problem becomes more pronounced when the properties of the material transition from a linear to a nonlinear response. Figure 7(a) shows a stress–strain curve typical

of polymeric materials. This figure illustrates the range of material behavior that must be described as one transition from small strains to ultimate failure when describing the behavior of polymer films undergoing indentation testing.

Several options are available for describing nonlinear material behavior in ANSYS. Two models were used for calculating the plasticity parameters in the present study. The first is a bilinear kinematic hardening model (BKIN). The relatively simple BKIN model is often used in large strain analysis. Using the bilinear model the material response is described in terms of three parameters; an elastic modulus ( $E$ ), a yield point ( $\sigma_y$ ) and a tangent modulus ( $E_T$ ) [see Figure 7(b)]. The back stress tensor for bilinear kinematic hardening evolves so that the effective stress versus effective strain curve is bilinear. The initial slope of the curve is the elastic modulus of the material and beyond the user specified initial yield stress ( $\sigma_y$ ), plastic strain develops and the back stress evolves to that stress versus total strain continues

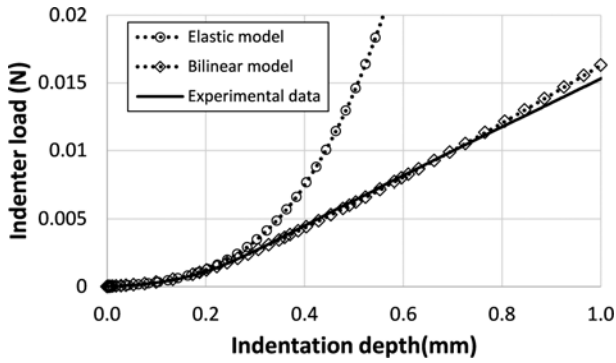


**Figure 8.** A 1 mm indentation depth was simulated with only elastic modulus ( $E$ ) and pre-strain ( $\varepsilon_0$ ), (open circles) and elastic modulus, pre-strain, yield strength ( $\sigma_y$ ) and tangent modulus (TanMod) (open diamonds). The elastic regime extends only about 200  $\mu\text{m}$  into the indentation. The bilinear model fits the data well for the depth shown, but deviations can already be seen near 0.8 mm indentation, and the difference increases with larger depth. Mechanical properties used for the simulation are  $E = 3.28 \text{ GPa}$ ,  $\varepsilon_0 = 0.0018$ ,  $\sigma_y = 43.50 \text{ MPa}$ ,  $\text{TanMod} = 100 \text{ MPa}$ .

along a line with slope defined by the user specified tangent modulus ( $E_T$ ). This tangent modulus cannot be less than zero or greater than the elastic modulus.

The second, more complicated, method of describing the relevant material response is through the use of a multilinear kinematic hardening model (KINH). In this case the stress-strain behavior is described by a series of linear functions, each characterized by individual stress ( $\sigma_n$ ) and its corresponding strain point  $\varepsilon_n$  [see Figure 7(c)]. The back stress tensor for multilinear kinematic hardening evolves so that the effective stress versus effective strain curve is multilinear with each of the linear segments defined by a set of user input stress-strain points.

For the optimization process on the plastic region, we used the elastic parameters from the elastic analysis and we calculate the yield strength and tangent modulus, Figure 8

shows the result of the optimization process, both for elastic parameters only as well as for the plastic parameters.

The figure shows that the bilinear model is most suitable for a small plastic deformation, where it is in good agreement with the data. For larger indentation depths, however, the difference between the model and the data increases substantially. In order to get indentation depth simulation of the order of 2 mm or higher, we used a multilinear kinematic hardening material model with stress-strain pairs. The model was developed by fitting the indentation data in small increments of 100  $\mu\text{m}$ . We begin with the elastic curve going up to a stress close to the yield point, and then begin the fit with an estimate for  $\varepsilon_1$  and  $\sigma_1$ . The output curve is compared with the data only up to the indentation depth than can be reached with  $\varepsilon_1$ . Once the error metric has been minimized for  $\varepsilon_1$  and  $\sigma_1$ , we fix those two values and move on  $\varepsilon_2$  and  $\sigma_2$ , thus gradually assembling the multilinear curve. ANSYS is able to handle up to 20 stress-strain points in the kinematic hardening material model. Figure 9(a) shows the indentation data and the optimized simulation, and Figure 9(b) shows the optimized material model for a 2.0 mm of indentation. It is a unique solution where the optimized material model shows features in the solution very similar to the typical polymer stress-strain curve depicted in Figure 7.

The multilinear model can be obtained for any indentation depth up to the failure depth, which was 3.7 mm for this specific sample. The multilinear model clearly explains why the bilinear model fails beyond 1 mm indentation range: the stress-strain curve changes slope at a strain of 0.5, which corresponds to about 1 mm of indentation depth. The curve also shows that the film fails at a strain of 0.9, remarkably large strain for a nonrubbery plastic. This large failure strain is reproducible and may be attributable to the low strain rates. The multilinear model also naturally adapts to the strain-softening feature around a strain of 0.02, where the

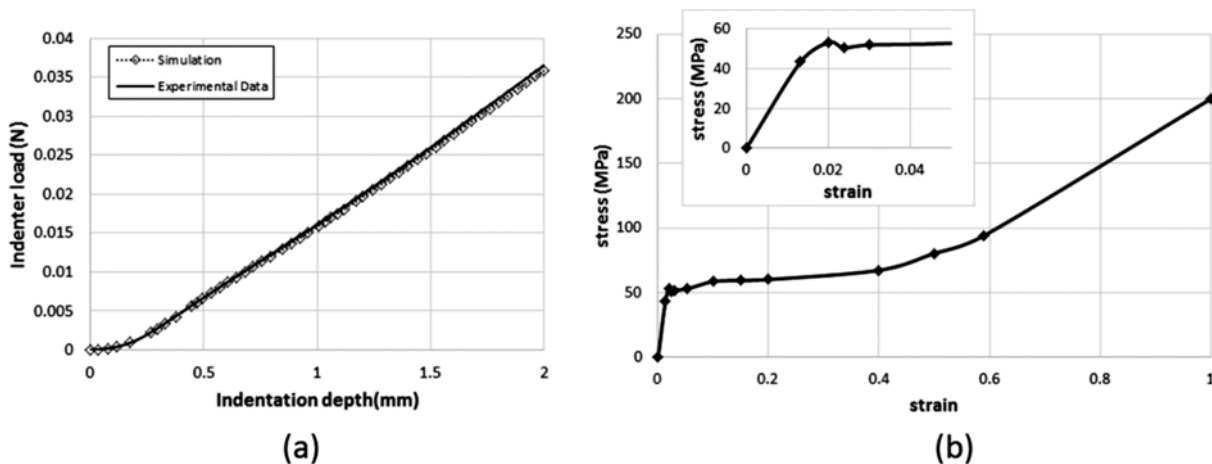


**Figure 9.** (a) 2 mm indentation simulation. The multilinear simulation result follows the data very well. (b) Optimized multilinear kinematic hardening material model for a film thickness of 100 nm. The inset shows the yield regime in greater detail. The points marked in diamonds on the plot are the points that were entered into the simulation.

slope of the stress–strain curve is briefly negative before leveling off and increasing again.

#### 4. Conclusions

A finite element model using ANSYS was created and an optimization script was developed in python to extract the material properties from indentation tests for ultra-thin films. The elastic regime was identified for indentation depths of 150–200  $\mu\text{m}$ , after which the film yields until failure. A bilinear material model is a good approach for indentation depths up to 1.0 mm. Beyond this depth, a multilinear model is required to get an accurate description of the experimental data. This method can be used to characterize mechanical properties for ultra-thin films that were fabricated under different conditions to find values that have hitherto eluded characterization, such as yield stress and failure strain.

#### Acknowledgements

This work was performed under the auspices of the U.S. Department of Energy by Lawrence Livermore National Laboratory under Contract DE-AC52-07NA27344. The work was funded by LLNL LDRD 14-ERD-025.

#### References

1. E. W. Liu H and S. Litster, *Langmuir* **31**, 9853 (2015).
2. S. Karan, Z. Jiang, and A. G. Livingston, *Science* **348**, 1347 (2015).
3. R. C. Trese M and M. J. Young, *Adv. Retinal Tissue Engng Mater.* **5**, 108 (2012).
4. B. Adhikari and S. Majumdar, *Progr. Polymer Sci.* **29**, 699 (2004).
5. J. D. Lindl, O. L. Landen, J. Edwards, *et al.*, *Phys. Plasmas* **21**, 020501 (2014).
6. S. R. Nagel, S. W. Haan, J. R. Rygg, C. Aracne-Ruddle, M. Barrios, L. R. Benedetti, D. K. Bradley, J. E. Field, B. A. Hammel, N. Izumi, O. S. Jones, S. F. Khan, T. Ma, A. E. Pak, K. Seagraves, M. Stadermann, R. J. Strauser, R. Tommasini, and R. P. J. Town, *Phys. Plasmas* **22**, 022704 (2015).
7. R. Tommasini, J. E. Field, B. A. Hammel, O. L. Landen, S. W. Haan, C. Aracne-Ruddle, L. R. Benedetti, D. K. Bradley, D. A. Callahan, E. L. Dewald, T. Doepfner, M. J. Edwards, O. A. Hurricane, N. Izumi, O. A. Jones, T. Ma, N. B. Meezan, S. R. Nagel, J. R. Rygg, K. S. Seagraves, M. Stadermann, R. J. Strauser, and R. P. J. Town, *Phys. Plasmas* **22**, 056315 (2015).
8. C. M. Stafford, B. D. Vogt, C. Harrison, D. Julthongpiput, and R. Huang, *Macromolecules* **39**, 5095 (2006).
9. J.-H. Lee, J. Y. Chung, and C. M. Stafford, *ACS Macro Lett.* **1**, 122 (2012).
10. W. Xia and S. Ketem, *J. Mater. Res.* **30**, 36 (2014).
11. Y. Liu, Y.-C. Chen, S. Hutchens, J. Lawrence, T. Emrick, and A. J. Crosby, *Macromolecules* **48**, 6534 (2015).
12. N. M. Bhatia and W. Nachbar, *AIAA J.* **6**, 1050 (1968).
13. M. Stadermann, S. O. Kucheyev, J. Lewicki, and S. A. Letts, *Appl. Phys. Lett.* **101**, 071908 (2012).
14. M. R. Begley and T. J. Mackin, *J. Mech. Phys. Solids* **52**, 2005 (2004).
15. M. Begley, O. Scott, U. Komaragiri, and T. Mackin, *Acta Mater.* **52**, 4877 (2004).
16. S. H. Baxamusa, M. Stadermann, C. Aracne-Ruddle, A. J. Nelson, M. Chea, S. Li, K. Youngblood, and T. I. Suratwala, *Langmuir* **30**, 5126 (2014).
17. M. Stadermann, S. H. Baxamusa, C. Aracne-Ruddle, M. Chea, S. Li, K. Youngblood, and T. I. Suratwala, *J. Vis. Exp.* (100), e52832 (2015).
18. E. Jones, T. Oliphant, and P. Peterson, *SciPy: Open Source Scientific Tools for Python* (2001), p. 2001.
19. W. M. H, *Proceedings of the 1995 Dundee Biennial Conference in Numerical Analysis* (1996), p. 191.
20. J. A. Nelder and R. Mead, *Comput. J.* **7**, 308 (1965).